



CHORUS

This is the accepted manuscript made available via CHORUS. The article has been published as:

Determination of spin Hall angle and spin diffusion length in β -phase-dominated tantalum

R. Yu, B. F. Miao, L. Sun, Q. Liu, J. Du, P. Omelchenko, B. Heinrich, Mingzhong Wu, and H. F. Ding

Phys. Rev. Materials **2**, 074406 — Published 23 July 2018

DOI: [10.1103/PhysRevMaterials.2.074406](https://doi.org/10.1103/PhysRevMaterials.2.074406)

1 Determination of spin Hall angle and spin diffusion length in β -phase dominated Tantalum

2 R. Yu¹, B. F. Miao^{1,2}, L. Sun^{1,2}, Q. Liu¹, J. Du^{1,2}, P. Omelchenko³, B. Heinrich³,

3 Mingzhong Wu⁴, H. F. Ding^{1,2*}

4 ¹*National Laboratory of Solid State Microstructures and Department of Physics, Nanjing University,*

5 *22 Hankou Road, Nanjing 210093, P. R. China*

6 ²*Collaborative Innovation Center of Advanced Microstructures, Nanjing University,*

7 *22 Hankou Road, Nanjing 210093, P. R. China*

8 ³*Department of Physics, Simon Fraser University, 8888 University Dr,*

9 *Burnaby, BC, Canada V5A 1S6*

10 ⁴*Department of Physics, Colorado State University, Fort Collins, CO 80523, USA*

11 *Corresponding author: hfding@nju.edu.cn

12

Abstract

1
2 The *dc* spin-to-charge conversions of Tantalum (Ta) in Ta/Co₄₀Fe₄₀B₂₀ bilayer structures are
3 investigated utilizing spin pumping and inverse spin Hall effects (ISHE). From Ta thickness
4 (t_{Ta})-dependent resistivity and X-ray diffraction measurements, we found that Ta films, below 30 nm
5 in thickness, are β -phase dominated. The damping enhancement shows a fast increase with t_{Ta} when
6 $t_{\text{Ta}} < 1$ nm and reaches a saturation value at ~ 1.5 nm. The ISHE induced charge voltages have
7 opposite signs for Ta and Pt. From t_{Ta} -dependent spin pumping produced ISHE voltage and
8 precession angle measurements, the normalized spin-charge conversion signal is found to increase
9 with t_{Ta} and saturate at ~ 15 nm. Our findings can be understood with a recently developed theory
10 [PRL 114,126602 (2015)], which includes spin backflow and a spin loss at the interface. With a fitted
11 spin loss factor of 0.02 ± 0.02 , we extract the spin Hall angle and spin diffusion length of high
12 resistivity Ta to be $\theta_{\text{SH}} = -0.0062 \pm 0.001$ and $\lambda_{\text{sd}} = 5.1 \pm 0.6$ nm, respectively.

13 **Keywords:** spin pumping, microwave photo-resistance, interface spin loss

1 Spintronics, a paradigm of electronics based on the spin degree of freedom of the electron, has
2 attracted increasing attention due to the advantages of being nonvolatile, reduced power dissipation,
3 and increased storage density as compared to traditional electronics devices [1-5]. Spintronics
4 initially emerged as the utilization of spin-polarized currents. Recently, spintronics entered a new
5 stage: exploration of pure spin currents. In comparison with spin-polarized currents, pure spin
6 currents are of more interest since they are accompanied by neither net charge currents nor stray
7 Oersted fields and can therefore carry information with minimal power dissipation [6,7]. Thus, it can
8 be anticipated that pure spin currents will play a crucial role in future spin-based electronic devices.
9 To integrate with current technology, which is mainly charge based, pure spin signals need to
10 interconvert efficiently with charge signals. The spin/charge current can interconvert to each other in
11 nonmagnetic materials by means of the spin Hall effect (SHE) or the inverse spin Hall effect (ISHE)
12 [5,8]. The conversion efficiency, typically characterized by the spin Hall angle (θ_{SH}), is thus one of
13 the key parameters for spintronics applications.

14 Various methods have been previously utilized to generate pure spin currents and estimate θ_{SH} ,
15 such as nonlocal spin injection [9], ferromagnetic resonance (FMR)-based spin pumping [10-13],
16 thermal spin injection [14], and spin torque FMR [15] etc. Among them, spin pumping is commonly
17 used in transition metals since their interfaces can be better characterized and be free from the
18 impedance mismatching issue [7,16]. Upon the microwave excitation, the magnetic moments in a
19 ferromagnet precess and inject a pure spin current \mathbf{J}_S , into an adjacent normal metal; and \mathbf{J}_S is
20 further converted into an electrical current \mathbf{J}_C via the ISHE through $\mathbf{J}_C = (2e/\hbar)\theta_{SH}\mathbf{J}_S \times \boldsymbol{\sigma}$, where
21 $\boldsymbol{\sigma}$ denotes the spin-polarization direction of \mathbf{J}_S , and \hbar is the reduced Planck constant. Generally,

1 large θ_{SH} is believed to exist in 4d and 5d transition metals [17]. Comparable θ_{SH} values were also
2 reported recently in alloys like CuBi [18], Permalloy [14], and 3d transition metals like Cr and Ni
3 [19]. Among those materials, β -Ta is of special interest as it has been predicted to have a large and
4 negative θ_{SH} [17]. A subsequent experiment also showed that β -Ta can serve as a material for high
5 efficiency magnetization switching [20]. Thus, the study of θ_{SH} in β -Ta attracts great interest.
6 Previously reported θ_{SH} of Ta vary largely, ranging from -0.0037 to -0.15 [20-28]. Therefore, a
7 systematical study to accurately determine the actual θ_{SH} is highly desired.

8 The discrepancy of the previously measured θ_{SH} may originate from the following reasons.
9 Firstly, during the spin pumping experiment, the detected voltage signal can include two components:
10 the ISHE voltage ($V_{\text{ISHE}}^{\text{SP}}$), and an unwanted signal which is typically related to anisotropic
11 magnetoresistance (AMR): V_{AMR} [10,12,29]. $V_{\text{ISHE}}^{\text{SP}}$ has a symmetrical Lorentzian line-shape
12 centered at the FMR field, H_r . In contrast, V_{AMR} can have both the anti-symmetrical and
13 symmetrical Lorentzian line-shape components also centered at H_r [29-32]. The presence of V_{AMR}
14 thus can influence the measurement of $V_{\text{ISHE}}^{\text{SP}}$. Therefore, the careful separation of these two signals is
15 necessary. Secondly, θ_{SH} by definition is the ratio of the spin to charge current before and after the
16 conversion. Thus, it is important to measure both spin and charge signals instead of the charge signal
17 alone. Most of the studies, however, assumed that the injected spin current has no dependence on the
18 thickness of the adjacent nonmagnetic film. It was recently reported that the precession angle, to
19 which the spin current is proportional, can depend on the thickness of the nonmagnetic layer even if
20 constant microwave power used [13]. Therefore, it is also important to measure the precession angles
21 for each individual sample [13,32,33]. Thirdly, the measurement of θ_{SH} is also connected with

1 another important material parameter, the spin diffusion length (λ_{sd}). λ_{sd} determines the length
2 scale of spin current transport [34] and defines the effective thickness for the spin-to-charge
3 conversion. Thus, a careful thickness dependent study is needed to quantify both θ_{SH} and λ_{sd} .
4 Fourthly, recent studies showed that the spin current may suffer a loss when flowing across an
5 interface and can therefore influence the determination of θ_{SH} and λ_{sd} [34-37]. So, a careful
6 characterization of the interface effect on the spin transport is also necessary.

7 In this study, we present a systematic study of θ_{SH} and λ_{sd} for β -phase dominated Ta by
8 taking into account all of the above-mentioned issues carefully. We used Ta/Co₄₀Fe₄₀B₂₀ (Ta/CoFeB)
9 bilayer samples. In combination the thickness dependent resistivity and X-ray diffraction (XRD)
10 measurements, we identified that the Ta films are mainly in β -phase when the film thickness is 30 nm
11 and less. Through the measurement of the spin pumping induced ISHE (SP-ISHE) signal at specially
12 chosen geometry, we excluded the AMR signal and obtained the pure ISHE signal [12,29]. With the
13 microwave photo-resistance measurements, the actual pumped spin current was characterized for
14 each individual sample by measuring the precession angles. To account for spin current transport at
15 the interface we measured t_{Ta} -dependence ($t_{Ta} < 2$ nm) of enhanced interface damping; the data was
16 analyzed by the recently developed model [36,37], allowing one to estimate the spin loss at the
17 interface. With all these efforts, we found $\theta_{SH} = -0.0062 \pm 0.001$ and $\lambda_{sd} = 5.1 \pm 0.6$ nm for
18 β -phase dominated Ta.

19 The Ta/CoFeB bilayers were grown on GaAs (001) substrate by *dc* magnetron sputter
20 deposition at room temperature. The base pressure of the chamber is 2×10^{-5} Pa. Prior to the growth,
21 the substrates are thoroughly rinsed sequentially with acetone, ethanol and deionized water in

1 ultrasonic water bath (100 W). During the growth, the Ar pressure is maintained at 0.3 Pa. The
2 growth conditions for the deposition of Ta are: 0.046 A for the current and 348 V for the applied
3 voltage. Ta growth rate is calibrated by an X-ray diffraction (XRD) to be ~ 0.111 nm/s. Immediately
4 after the growth of the Ta film, we grow the CoFeB film on top of the Ta film in the same chamber
5 with the conditions of the 0.06 A for the current and 396 V for the voltage. The calibrated growth rate
6 for CoFeB is ~ 0.176 nm/s. The distance between the target and the substrate is fixed at ~ 65 mm for
7 both Ta and CoFeB. The bilayers are patterned into stripes with the width of $w = 20 \mu\text{m}$ and
8 length of $L = 1820 \mu\text{m}$ through photolithography and lift-off techniques. Figure 1(a) shows the
9 sketch of the device used for the measurements. The light blue rectangles are the signal line (S) and
10 the ground lines (G) of a coplanar waveguide (CPW). The purple long stripe represents the sample
11 that is placed in the center between S and G lines. In this structure, the microwave magnetic field
12 \vec{h}_{rf} is mainly perpendicular to the sample plane and along the z -direction [29]. A network analyzer
13 with the variable frequency: f in the range of 20 MHz to 20 GHz was used to generate a microwave
14 power for spin pumping induced ISHE and FMR measurements. A rotatable dc magnetic field \vec{H}
15 with tunable magnitude was applied within the sample plane. The angle between \vec{H} and the bilayer
16 stripe, α_0 can be controlled through a servo-motor with high accuracy (error margin $< 0.15^\circ$). In the
17 measurements, the resistance of the stripe is measured with the four probes method and the voltage
18 generated by spin pumping is detected as the function of \vec{H} via the two contact bars placed at both
19 ends of the stripes. To increase the signal to noise ratio, a lock-in amplifier was used in the
20 configuration of the amplitude modulation of the microwave signal and a frequency 51.73 kHz. All
21 the measurements were performed at room temperature. Figure 1(b) shows a schematic illustration of

1 the spin current transport across the interface (black) between ferromagnetic (green) and normal
 2 (yellow) layer. On the left, the spin current is transmitted through the interface without any loss. On
 3 the right, the spin current suffers an interface spin loss during the transmission, and only a part of the
 4 pumped spin current enters the nonmagnetic layer and is further converted into the charge current
 5 due to ISHE.

6 Tantalum has $5d^36s^2$ outer shell electrons and is less than half-filled in d-orbits. Therefore, it is
 7 anticipated to have a negative spin Hall angle [17], in contrast to the positive one reported for Pt
 8 ($4d^96s^1$). Figure 2(a) shows the measured voltage as the function of \vec{H} for both the Pt and Ta layers.
 9 The green circles are for Ta (5)/CoFeB(10) (the numbers in brackets are the layer thickness in nm)
 10 and the black squares are for Pt (5)/CoFeB (10). The solid red lines are the fits utilizing the
 11 symmetric Lorentzian line-shape. Both measurements are taken at 8 GHz. In order to eliminate the
 12 unwanted V_{AMR} , we followed our previous approach [12,29] and chose two special geometries, i.e.,
 13 $\alpha_0 = 90^\circ$ and $\alpha_0 = 270^\circ$ (not shown) according to their different dependences on the angle α_0 :
 14 $V_{ISHE}^{SP} \propto \sin \alpha_0$ and $V_{AMR} \propto \sin 2\alpha_0$. As shown in Fig. 2(a), the experimental data can be fit well by
 15 the symmetric Lorentzian line shape (red curves). The signals are inverted for the same sample for
 16 $\alpha_0 = 90^\circ$ and $\alpha_0 = 270^\circ$ (not shown). The almost perfect fit with symmetrical Lorentzian line shape
 17 and the sign inversion at $\alpha_0 = 90^\circ$ and $\alpha_0 = 270^\circ$ evidence that the measured signals are pure
 18 ISHE signals caused by spin pumping. Notice, the *dc* voltage signals obtained for Ta and Pt are
 19 indeed opposite in sign, as predicted theoretically [17].

20 As mentioned above, the measured V_{ISHE}^{SP} in real experiments is often mixed with V_{AMR} . When
 21 the angle α_0 is not exactly equal to 90° or 270° , the measured voltage for Ta (5)/CoFeB (10)

1 bilayer can contain both symmetric and anti-symmetric signal due to the mixing with V_{AMR} . To
 2 illustrate this effect, we show the signal obtained at a slightly tilted angle, $\alpha_0 = 89^\circ$ in Fig. 2(b).
 3 Interestingly, the measured voltage is no longer purely symmetrical even though α_0 is only tilted
 4 away by 1° from 90° . Our fits yield the anti-symmetrical component (solid blue line) to be $\sim 4 \mu\text{V}$,
 5 which is $\sim 40\%$ of $\sim 9 \mu\text{V}$ obtained for the symmetrical component (solid red line). We note that a
 6 similar effect is also observed by M. Obstbaum et al [38]. Therefore, ISHE study requires highly
 7 accurate alignment of the sample geometry to obtain the pure and non-contaminated ISHE voltage
 8 signal.

9 Ta films grown by sputtering can form two different crystalline phases, the bcc phase (α -Ta) and
 10 the tetragonal phase (β -Ta). These two phases were reported to have significantly different resistivity
 11 in ref. [39]. This difference was also confirmed by several experiments [40-42]. Though the exact
 12 resistivity depends on the substrate and the growth conditions, it is generally accepted that the
 13 resistivity is $15 - 50 \mu\Omega \cdot \text{cm}$ for α -Ta and $140 - 220 \mu\Omega \cdot \text{cm}$ for β -Ta, respectively. To determine
 14 the resistivity of our Ta films, deposited on top of GaAs substrates, we measured the resistance for Ta
 15 (t_{Ta}) with t_{Ta} varied in the range of 2-55 nm with four probes method. The results are shown in Fig.
 16 3(a). The t_{Ta} dependent ρ_{Ta} shows a large value of $400 \mu\Omega \cdot \text{cm}$ at 2 nm, a fast decrease when $t_{\text{Ta}} <$
 17 15 nm and a slow decrease for $t_{\text{Ta}} > 15 \text{ nm}$. To obtain quantitative information, we fit our results with
 18 a semi-classical Fuchs-Sondheimer model [43], $\rho_{\text{Ta}} = \rho_0 [1 - (\frac{1}{2} + \frac{3\lambda_{\text{mf}}}{4t_{\text{Ta}}})(1 - pe^{-t_{\text{Ta}}\xi/\lambda_{\text{mf}}})e^{-t_{\text{Ta}}/\lambda_{\text{mf}}}]^{-1}$ with
 19 $t_{\text{Ta}}/\lambda_{\text{mf}} > 0.1$. In it, ρ_0 represents the bulk resistivity, λ_{mf} stands for the electron mean free path,
 20 while p and ξ are the surface scattering and the grain boundary scattering parameters, respectively.

1 The fit (blue line) reproduces the experimental data and yields $\lambda_{\text{mf}} = 10 \pm 4 \text{ nm}$, $p = 0.9 \pm 0.03$,
 2 $\xi = 0.6 \pm 0.2$ and $\rho_0 = 130 \pm 9 \mu\Omega \cdot \text{cm}$. We found that the measured resistivity was larger than 140
 3 $\mu\Omega \cdot \text{cm}$ in the thickness range of 2-30 nm, indicating that the films in this thickness range are
 4 dominated by β -Ta phase [26,44]. In addition, when we limited our fitting range to 2-30 nm (red line),
 5 the extrapolated values change to $\lambda_{\text{mf}} = 7 \pm 4 \text{ nm}$, $p = 0.9 \pm 0.06$, $\xi = 0.6 \pm 0.2$ and
 6 $\rho_0 = 139 \pm 13.6 \mu\Omega \cdot \text{cm}$. The extrapolated bulk resistivity is very close to the value of β -Ta
 7 suggesting that β -Ta is dominant when the thickness is below 30 nm. To further confirm this, we
 8 performed the XRD measurements. As shown in Fig. 3(b), the Ta films with thicknesses 20/30/40/50
 9 nm were dominated by the tetragonal β -Ta phase since a strong peak corresponding to the Bragg
 10 diffraction peak (002) of β -Ta was found. In the large thickness region, namely at thickness of 40/50
 11 nm, we also observe a weak peak corresponding to the (110) Bragg diffraction peak of α -Ta in good
 12 agreement with previous findings [44]. As shown in the inserted amplified view, we did not observe
 13 any α -Ta peak for the films with the thickness of 30 nm and less, which is consistent with the
 14 resistivity measurements indicating films mainly in β -phase. Thus, we can conclude that our
 15 deposited Ta films are indeed dominated by the β -phase in the thickness below 30 nm and we will
 16 limit our discussion of the spin pumping induced ISHE measurements in this range.

17 In the following, we discuss the method for estimating the magnitude of the pumped spin
 18 current. According to the spin pumping theory [45], the pumped spin current is proportional to the
 19 product of the in- and out-of-plane precession angles. At the resonance condition,
 20 $j_s^0(H_r) \propto g_{\text{eff}}^{\uparrow\downarrow} f \alpha_1 \beta_1$, where $g_{\text{eff}}^{\uparrow\downarrow}$ is the effective spin mixing conductance parameter, and α_1, β_1 are
 21 the in- and out-of-plane precession angles at the resonance field, respectively. Therefore, an accurate

1 characterization of the precession angles is also crucial for the estimation of the magnitude of the
 2 pumped spin current and the calculation of θ_{SH} . This crucial step, however, is ignored in many
 3 studies where it is often assumed that a given microwave power always yields the same \vec{h}_{rf} in the
 4 sample. With the microwave photo-resistance measurements, recent studies showed that the
 5 precession angle can change when the thickness of Pd layer is varied in Py/Pd [13]. The method was
 6 originally used to study the spin rectification effect [30] and was recently adopted for the spin
 7 pumping study [12]. The validity of the method is further confirmed by Ref. [32] where different
 8 methods were compared and only this method can warrant the frequency independence of the spin
 9 Hall angle. We continued using this method to estimate α_1 and β_1 for each individual sample. Figure
 10 4 presents t_{Ta} dependence of α_1 at $\alpha_0 = 90^\circ$ with the microwave of $f = 10$ GHz with amplitude of
 11 -18 dBm combined with a microwave amplifier with the gain of 200. The typical microwave
 12 photo-resistance measurement is shown in the inset utilizing Ta (20)/CoFeB (10) as an example. The
 13 black circles are the experiment data, and the solid red line is the fit utilizing symmetrical Lorentzian
 14 function. The amplitude at H_f is used to calculate α_1 for each individual sample and a t_{Ta} dependence
 15 is obtained. We found that α_1 increased with t_{Ta} up to 15 nm and then remained almost constant with
 16 further increasing t_{Ta} . The result confirms that the precession angle is indeed not a constant for
 17 different samples even when they are excited with the same input microwave power. Thus, the
 18 careful measurement of the precession angles for each sample is necessary in the quantitative
 19 estimation of θ_{SH} as we did for Ta in this study.

20 Damping enhancement ($\Delta\alpha = \alpha_{\text{F/N}} - \alpha_{\text{F}}$, where $\alpha_{\text{F/N}}$ is the total damping for F/N bilayer and α_{F}
 21 is the damping for single F layer) is the main character of spin pumping [45]. It also contains the

1 information of the absorption of spin current at the interface [36,37]. Therefore, the enhancement of
2 damping can be used to characterize the influence of the interface on the transportation of spin
3 current. With the FMR measurements, we obtain the damping parameter α by using the slope of
4 FMR linewidth as a function of microwave frequency. Further, we can calculate the effective spin
5 mixing conductance, $g_{\text{eff}}^{\uparrow\downarrow}$ according to $g_{\text{eff}}^{\uparrow\downarrow} = (4\pi M_S t_F / g\mu_B)(\alpha_{F/N} - \alpha_F)$, where M_S is the saturate
6 magnetization and t_F is the thickness of the FM layer. To further illustrate the interface effect, the
7 measurements with $t_{\text{Ta}} < 2$ nm were taken from a series of samples made by a wedge-shape growth
8 technique. Figure 5(a) illustrates $g_{\text{eff}}^{\uparrow\downarrow}$ as the function of t_{Ta} . To highlight the change at $t_{\text{Ta}} < 2$ nm,
9 we also show the amplified view in the inset for the small thickness range. We find that $g_{\text{eff}}^{\uparrow\downarrow}$ has a
10 fast increase when $t_{\text{Ta}} < 2$ nm and reaches a saturation value at $t_{\text{Ta}} \sim 1.5$ nm. The result is similar with
11 previous study where a saturation thickness of ~ 2 nm was reported [46]. As mentioned above, we can
12 exclude most of the unwanted spin rectification effect and obtained the ISHE signal at the special
13 chosen geometries, namely at $\alpha_0 = 90^\circ, 270^\circ$. To further eliminate the residual spin rectification
14 effect, we measured SP-ISHE and the microwave photo-resistance effect at both geometries in the
15 same setup and redefined a normalized ISHE voltage induced by spin pumping

16 $\tilde{V}_{\text{ISHE}}^{\text{SP}}(H_r) = \left[\frac{V}{\alpha_1 \beta_1} \Big|_{\alpha_0=90^\circ} - \frac{V}{\alpha_1 \beta_1} \Big|_{\alpha_0=270^\circ} \right] / 2$. Together with the measured $g_{\text{eff}}^{\uparrow\downarrow}$ and the Ta resistance R_N

17 for each individual sample, we plot the thickness dependent $\frac{\tilde{V}_{\text{ISHE}}^{\text{SP}}(H_r)}{ewfR_N}$ in Fig. 5(b). The black
18 squares and the red circle represent data obtained at the frequencies of 9 GHz and 10 GHz,
19 respectively. All the ISHE data is negative in the thickness range that we investigated. The signal
20 shows a decrease with increasing thickness and reaches a saturation at $t_{\text{Ta}} \approx 20$ nm. Comparing with

1 the measured t_{Ta} dependent $g_{\text{eff}}^{\uparrow\downarrow}$ shown in Fig. 4(a), we found that two signals reach their saturation
 2 values at very different thicknesses. Namely, one is at ~ 1.5 nm and the other is at ~ 20 nm. This
 3 dramatic difference was also reported in the Py/Pt system [12] and Co/Pt system [35]. A possible
 4 explanation is the spin loss at the interface [35-37,47]. It suggests that the pumped pure spin current
 5 not only transmits and reflects at the F/N interface but also suffers a loss, the interface spin loss, as
 6 shown in the right panel of Fig. 1(b).

7 The spin loss at the interface was originally introduced in the study of
 8 current-perpendicular-to-plane (CPP) giant magneto-resistance [48,49]. Rojas-Sánchez *et al.*
 9 combined the spin diffusion model with spin pumping measurements to study the spin pumping
 10 induced ISHE in Co/Pt system [35] to show the important role of spin memory loss at the interface.
 11 First-principles calculations confirm that a considerable part of the pumped spin current dissipates at
 12 the Py/Pt interface [50]. Zhang *et al.* also described the spin loss utilizing a parameter denoting the
 13 transparency of the interface in the investigation the spin-charge conversion in Pt [47]. Chen and
 14 Zhang revisited spin pumping theory including spin-orbit coupling (SOC) at the interface and found
 15 a discontinuity in the spin current at the interface [37]. The interface spin loss provides a possible
 16 explanation for $g_{\text{eff}}^{\uparrow\downarrow}$ and $\frac{\tilde{V}_{\text{ISHE}}^{\text{SP}}(H_r)}{ewfR_N}$ having different approaches to saturation with the increasing
 17 thicknesses of the nonmagnetic layer. Interestingly, the theory by Chen and Zhang only requires
 18 careful thickness dependent measurements of $g_{\text{eff}}^{\uparrow\downarrow}$ and $\frac{\tilde{V}_{\text{ISHE}}^{\text{SP}}(H_r)}{ewfR_N}$ to estimate the spin loss at the
 19 interface. It doesn't need additional measurements for extra parameters such as the interfacial
 20 resistance.

1 We used this model to analyze our experimental data. For the reader's convenience, we briefly
 2 summarize the model here. The essential assumption is that every time the spin current crosses the
 3 FM/NM interface, it loses its amplitude by a factor of δ and only $(1-\delta)J_s$ crosses the interface
 4 [36,37,51]. Since the backflow spin current [51] has to cross the interface twice, firstly on the way
 5 into nonmagnetic layer and secondly on the way getting back to the ferromagnetic layer, the effective
 6 spin mixing conductance thus can be written as:

$$7 \quad g_{\text{eff}}^{\uparrow\downarrow} = G^{\uparrow\downarrow} [1 - (1-\delta)^2 \varepsilon] \quad (1)$$

8 where $\varepsilon = G^{\uparrow\downarrow} / (G^{\uparrow\downarrow} + \frac{2}{3} k_F^2 \frac{\lambda_{\text{mf}}}{\lambda_{\text{sd}}} \tanh \frac{t_{\text{N-}}}{\lambda_{\text{sd}}})$ characterizes the back-flow spin current, k_F is the Fermi
 9 vector of NM layer. The model also estimates the transmitted pure spin current and the loss at the
 10 interface to be $G^{\uparrow\downarrow}(1-\varepsilon)(1-\delta)$ and $G^{\uparrow\downarrow}(1+\varepsilon-\varepsilon\delta)\delta$, respectively. The transmitted pure spin
 11 current is converted to the charge current via ISHE. Meanwhile the lost pure spin current can also
 12 contribute an additional charge voltage via the inverse Edelstein Effect [52,53]. By summing up both
 13 contributions together, the total converted charge signal can be written as:

$$14 \quad \frac{\tilde{V}_{\text{ISHE}}^{\text{SP}}(H_r)}{ewfR_{\text{N}}} = G^{\uparrow\downarrow}(1-\varepsilon)(1-\delta)\theta_{\text{SH}}\lambda_{\text{sd}} \tanh\left(\frac{t_{\text{N-}}}{2\lambda_{\text{sd}}}\right) + \lambda_{\text{IEE}}G^{\uparrow\downarrow}(1+\varepsilon-\varepsilon\delta)\delta \quad (2)$$

15 where λ_{IEE} is known as the inverse Edelstein length [36,37].

16 We took Eqs. (1) and (2) to fit our experimental data in the thickness range of 2-30 nm since we
 17 found that Ta is dominated by the β -phase in this range. The data above 30 nm are presented only to
 18 double check the measured effective spin mixing conductance and spin pumping induced ISHE
 19 signal reach their saturation. In the fits, we chose a literature value of $k_F = 11.8 \text{ nm}^{-1}$ reported in Ref.
 20 [27]. To further minimize the number of parameters in the whole fitting process, we take two steps to

1 fit the experimental data in Fig. 5(a) and Fig. 5(b). Firstly, we use a fixed test value for λ_{mf} and λ_{sd}
 2 to fit $G^{\uparrow\downarrow}$ and δ for the measured $G_{\text{eff}}^{\uparrow\downarrow} \sim t_{\text{N}}$ data according to Eq. (1). With the extracted values of
 3 $G^{\uparrow\downarrow}$ and δ , we continue to fit $\frac{\tilde{V}_{\text{ISHE}}^{\text{SP}}(H_{\text{r}})}{e\omega f R_{\text{N}}} \sim t_{\text{N}}$ data according to Eq. (2) to obtain θ_{SH} and λ_{sd} . We
 4 repeated these two fitting steps with the newly obtained λ_{sd} until a convergence is reached. We find
 5 the curves can be best fitted with $\lambda_{\text{mf}} = 3.7 \text{ nm}$, which lies in-between the error margin gives by
 6 Fuchs-Sondheimer theory ($7 \pm 4 \text{ nm}$), and larger than Drude model (0.64 nm). In Fig. 5(a) and its
 7 inset, the resulting fits are plotted as the red lines. It can be found that the fits reproduce the
 8 experimental data well. The fits also yield $G^{\uparrow\downarrow} = (1.17 \pm 0.07) \times 10^{19} \text{ m}^{-2}$ and a small spin loss
 9 factor δ of 0.02 ± 0.02 . The small spin loss is consistent with the value about 0.049 adopted for the
 10 same system by Cecot et al. [54] using the spin diffusion model [48]. The experimentally obtained
 11 t_{Ta} -dependent voltage signal can also be well described by Chen and Zhang's theory as shown in Fig.
 12 5(b), where the black/red lines represent the fits for 9 GHz and 10 GHz, respectively. The fits yield
 13 $\theta_{\text{SH}} = -0.0064 \pm 0.001$, $\lambda_{\text{sd}} = 4.8 \pm 0.6 \text{ nm}$, and $\lambda_{\text{IEE}} = 0.06 \pm 0.09 \text{ nm}$ for 9 GHz;
 14 $\theta_{\text{SH}} = -0.0060 \pm 0.0007$, $\lambda_{\text{sd}} = 5.3 \pm 0.5 \text{ nm}$ and $\lambda_{\text{IEE}} = 0.06 \pm 0.07 \text{ nm}$ for 10 GHz. By averaging
 15 these two values, we obtained $\theta_{\text{SH}} = -0.0062 \pm 0.001$ and $\lambda_{\text{sd}} = 5.1 \pm 0.6 \text{ nm}$ for β -phase
 16 dominated Ta. We also obtained $\lambda_{\text{IEE}} = 0.06 \pm 0.08 \text{ nm}$ which is close to zero. The interface spin
 17 loss for CoFeB-Ta is tiny, i.e. the interface is highly transparent for spin current, indicating that the
 18 interface Rashba spin-orbit interaction is not large. In addition, The value of λ_{IEE} not only depends
 19 the Rashba spin-orbit interaction, but also influenced by the interface disorder [36]. Since our
 20 bilayers are fabricated by sputtering, interfacial disorder is expected and the inverse Edelstein effect

1 could be strongly suppressed resulting in the small value of λ_{IEE} . If the interface is sharper, for
2 instance, layer-by-layer growth by molecular beam epitaxy, we would expect a larger λ_{IEE} value in
3 that case.

4 In the following, we make a brief comparison of our data with previous studies. Interestingly,
5 we found our measured spin Hall angle and spin diffusion length are in good agreement with those
6 extracted from lateral spin valve geometry in Ref. [55] where $\theta_{\text{SH}} = -0.008 \pm 0.002$ and
7 $\lambda_{\text{sd}} = 3 \pm 0.4$ nm were reported. Our results are also in good agreement with the values of
8 $G^{\uparrow\downarrow} = 1.4 \times 10^{19} \text{ m}^{-2}$, $\theta_{\text{SH}} = -0.005$ and $\lambda_{\text{sd}} = 2.5$ nm reported in Ref. [25] even though the authors
9 made the assumption that the relative ratio between the symmetric/antisymmetric signals in spin
10 rectification effect are the same for CoFeB and CoFeB/Ta. Interestingly, the same authors refined the
11 value of spin Hall angle to -0.02 ± 0.0007 but they assumed the symmetrical component of the
12 measured signal originates from the spin pumping induced ISHE only [28]. A similar system was
13 also studied by Jamali et al. [24] using with spin pumping and a different value of spin Hall angle,
14 -0.014 , was reported. The difference may be due to the fact that their sample was annealed at a
15 temperature above 200 °C while our samples are grown at room temperature and without any
16 annealing. Evidence of the difference in samples between our study and Jamali et al. [24] can also be
17 observed in the significantly different effective spin mixing conductance. The spin Hall angle of Ta
18 in Ta/CoFeB was also studied by spin transfer torque FMR and much larger values were reported.
19 Generally, the spin Hall angle obtained by spin transfer torque FMR is about one order of magnitude
20 larger than the one measured by spin pumping, as reported for the Pt as well [20]. The reason is not
21 well understood at the present stage and deserves further investigation.

1 In summary, we studied the *dc* electron transport and spin pumping-induced ISHE in an
2 important class of Ta thin films playing a crucial role in spin pumping current transport and spin
3 torque devices. Together with the t_{Ta} -dependent resistivity and XRD measurements we found that in
4 our region of interest for our study, $2 < t_{\text{Ta}} < 30$ nm, the dominating structure of Ta is β -phase.
5 Through the t_{Ta} -dependent microwave photo-resistance measurements, we found that the precession
6 angles are different for films with different t_{Ta} even with the same input microwave power. Thus, to
7 quantify the pumped pure spin current, the precession angle characterization for each individual
8 sample is needed. Together with t_{Ta} -dependent effective spin mixing conductance and ISHE voltage
9 measurements as well as the interface spin loss described by Chen and Zhang [36,37], we obtain
10 consistent values of $\theta_{\text{SH}} = -0.0062 \pm 0.001$ and $\lambda_{\text{sd}} = 5.1 \pm 0.6$ nm at two different microwave
11 frequencies of 9 and 10 GHz.

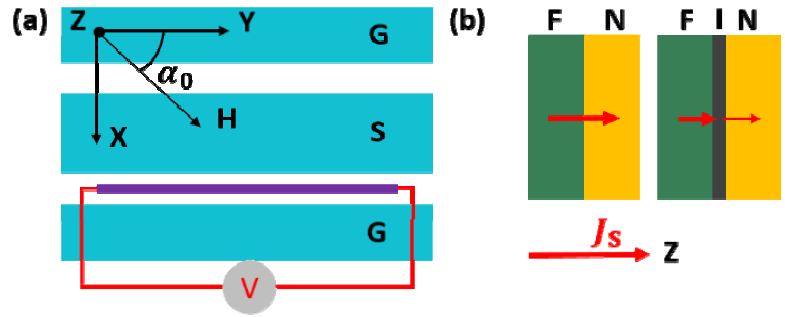
12 This work was supported by the National Key R&D Program of China (Grant No.
13 2017YFA0303202), the National Natural Science Foundation of China (Grants No. 51571109, No.
14 11734006, No. 51601087, No. 11374145, and No. 51471085), the Natural Science Foundation of
15 Jiangsu Province (Grant No. BK20150565), and the Fundamental Research Funds for the Central
16 Universities (Grant No. 14380078). M.W. was supported by the SHINES, an Energy Frontier
17 Research Center funded by the U.S. Department of Energy (SC0012670), and the U.S. National
18 Science Foundation (EFMA-1641989, DMR-1407962). P. O. and B. H. was supported by the Natural
19 Sciences and Engineering Research Council of Canada (NSERC).

1 References:

- 2 [1] S. A. Wolf, D. D. Awschalom, R. A. Buhrman, J. M. Daughton, S. von Molnár, M. L. Roukes, A.
3 Y. Chtchelkanova, and D. M. Treger, *Science* **294**, 1488 (2001).
4 [2] Y. Tserkovnyak, A. Brataas, G. E. Bauer, and B. I. Halperin, *Rev. Mod. Phys.* **77**, 1375 (2005).
5 [3] S. D. Bader, *Rev. Mod. Phys.* **78**, 1 (2006).
6 [4] S. Bader and S. Parkin, *Annu. Rev. Condens. Matter Phys.* **1**, 71 (2010).
7 [5] J. Sinova, S. O. Valenzuela, J. Wunderlich, C. Back, and T. Jungwirth, *Rev. Mod. Phys.* **87**, 1213
8 (2015).
9 [6] S. Murakami, N. Nagaosa, and S.-C. Zhang, *Science* **301**, 1348 (2003).
10 [7] S. Maekawa, SO Valenzuela, E. Saitoh, and T. Kimura, (Oxford University Press, Oxford, 2012).
11 [8] S. Maekawa, H. Adachi, K.-i. Uchida, J. i. Ieda, and E. Saitoh, *J. Phys. Soc. Jpn.* **82**, 102002
12 (2013).
13 [9] S. O. Valenzuela and M. Tinkham, *Nature* **442**, 176 (2006).
14 [10] E. Saitoh, M. Ueda, H. Miyajima, and G. Tatara, *Appl. Phys. Lett.* **88**, 182509 (2006).
15 [11] O. Mosendz, J. Pearson, F. Fradin, G. Bauer, S. Bader, and A. Hoffmann, *Phys. Rev. Lett.* **104**,
16 046601 (2010).
17 [12] Z. Feng *et al.*, *Phys. Rev. B.* **85**, 214423 (2012).
18 [13] X. Tao, Z. Feng, B. Miao, L. Sun, B. You, D. Wu, J. Du, W. Zhang, and H. Ding, *J. Appl. Phys.*
19 **115**, 17C504 (2014).
20 [14] B. Miao, S. Huang, D. Qu, and C. Chien, *Phys. Rev. Lett.* **111**, 066602 (2013).
21 [15] L. Liu, T. Moriyama, D. Ralph, and R. Buhrman, *Phys. Rev. Lett.* **106**, 036601 (2011).
22 [16] S. Jiang, S. Liu, P. Wang, Z. Luan, X. Tao, H. Ding, and D. Wu, *Phys. Rev. Lett.* **115**, 086601
23 (2015).
24 [17] T. Tanaka, H. Kontani, M. Naito, T. Naito, D. S. Hirashima, K. Yamada, and J. Inoue, *Phys. Rev.*
25 **B. 77**, 165117 (2008).
26 [18] Y. Niimi, Y. Kawanishi, D. Wei, C. Deranlot, H. Yang, M. Chshiev, T. Valet, A. Fert, and Y.
27 Otani, *Phys. Rev. Lett.* **109**, 156602 (2012).
28 [19] H. Wang, C. Du, Y. Pu, R. Adur, P. C. Hammel, and F. Yang, *Phys. Rev. Lett.* **112**, 197201
29 (2014).
30 [20] L. Liu, C.-F. Pai, Y. Li, H. Tseng, D. Ralph, and R. Buhrman, *Science* **336**, 555 (2012).
31 [21] M. Morota, Y. Niimi, K. Ohnishi, D. Wei, T. Tanaka, H. Kontani, T. Kimura, and Y. Otani, *Phys.*
32 *Rev. B.* **83**, 174405 (2011).
33 [22] P. Deorani and H. Yang, *Applied Physics Letters* **103**, 232408 (2013).
34 [23] C. Hahn, G. De Loubens, O. Klein, M. Viret, V. V. Naletov, and J. B. Youssef, *Phys. Rev. B.* **87**,
35 174417 (2013).
36 [24] M. Jamali, A. Klemm, and J.-P. Wang, *Appl. Phys. Lett.* **103**, 252409 (2013).
37 [25] D.-J. Kim, S.-I. Kim, S.-Y. Park, K.-D. Lee, and B.-G. Park, *Curr. Appl. Phys* **14**, 1344 (2014).
38 [26] D. Qu, S. Huang, B. Miao, S. Huang, and C. Chien, *Phys. Rev. B.* **89**, 140407 (2014).
39 [27] G. Allen, S. Manipatruni, D. E. Nikonov, M. Doczy, and I. A. Young, *Phys. Rev. B.* **91**, 144412
40 (2015).

1 [28]S.-I. Kim, D.-J. Kim, M.-S. Seo, B.-G. Park, and S.-Y. Park, Appl. Phys. Lett. **106**, 032409
2 (2015).
3 [29]L. Bai, Z. Feng, P. Hyde, H. Ding, and C.-M. Hu, Appl. Phys. Lett. **102**, 242402 (2013).
4 [30]N. Mecking, Y. Gui, and C.-M. Hu, Phys. Rev. B. **76**, 224430 (2007).
5 [31]A. Azevedo, L. Vilela-Leão, R. Rodríguez-Suárez, A. L. Santos, and S. Rezende, Phys. Rev. B.
6 **83**, 144402 (2011).
7 [32]S. Gupta, R. Medwal, D. Kodama, K. Kondou, Y. Otani, and Y. Fukuma, Appl. Phys. Lett. **110**,
8 022404 (2017).
9 [33]M. Kavand, C. Zhang, D. Sun, H. Malissa, Z. Vardeny, and C. Boehme, Phys. Rev. B. **95**,
10 161406 (2017).
11 [34]J. Bass and W. P. Pratt Jr, J. Phys. Condens. Matter. **19**, 183201 (2007).
12 [35]J.-C. Rojas-Sánchez *et al.*, Phys. Rev. Lett. **112**, 106602 (2014).
13 [36]K. Chen and S. Zhang, Phys. Rev. Lett. **114**, 126602 (2015).
14 [37]K. Chen and S. Zhang, IEEE. Mag. Lett. **6**, 1 (2015).
15 [38]M. Obstbaum, M. Härtinger, H. Bauer, T. Meier, F. Swientek, C. Back, and G. Woltersdorf, Phys.
16 Rev. B. **89**, 060407 (2014).
17 [39]M. H. Read and C. Altman, Appl. Phys. Lett **7**, 51 (1965).
18 [40]J. J. Senkevich, T. Karabacak, D.-L. Bae, and T. S. Cale, J. Vac. Sci. Technol. B. **24**, 534 (2006).
19 [41]M. Grosser and U. Schmid, Thin solid films **517**, 4493 (2009).
20 [42]M. Shiojiri, S. Shinkai, K. Sasaki, H. Yanagisawa, and Y. Abe, Jpn. J. Appl. Phys **42**, 4499
21 (2003).
22 [43]P. Fan, K. Yi, J.-D. Shao, and Z.-X. Fan, J. Appl. Phys. **95**, 2527 (2004).
23 [44]E. Montoya, P. Omelchenko, C. Coutts, N. R. Lee-Hone, R. Hübner, D. Broun, B. Heinrich, and
24 E. Girt, Phys. Rev. B. **94**, 054416 (2016).
25 [45]Y. Tserkovnyak, A. Brataas, and G. E. Bauer, Phys. Rev. Lett. **88**, 117601 (2002).
26 [46]A. Conca, B. Heinz, M. Schweizer, S. Keller, E. T. Papaioannou, and B. Hillebrands, Phys. Rev.
27 B. **95**, 174426 (2017).
28 [47]W. Zhang, W. Han, X. Jiang, S.-H. Yang, and S. S. Parkin, Nat.Phys. **11**, 496 (2015).
29 [48]A. Fert and S.-F. Lee, Phys. Rev. B. **53**, 6554 (1996).
30 [49]D. V. Baxter, S. Steenwyk, J. Bass, and W. Pratt Jr, J. Appl. Phys. **85**, 4545 (1999).
31 [50]Y. Liu, Z. Yuan, R. J. Wesselink, A. A. Starikov, and P. J. Kelly, Phys. Rev. Lett. **113**, 207202
32 (2014).
33 [51]H. Jiao and G. E. Bauer, Phys. Rev. Lett. **110**, 217602 (2013).
34 [52]G. Bihlmayer, Y. M. Koroteev, P. Echenique, E. Chulkov, and S. Blügel, Surf. Sci. **600**, 3888
35 (2006).
36 [53]J. R. Sánchez, L. Vila, G. Desfonds, S. Gambarelli, J. Attané, J. De Teresa, C. Magén, and A.
37 Fert, Nat. Commun. **4**, 2944 (2013).
38 [54]M. Cecot *et al.*, Sci. Rep. **7**, 968 (2017).
39 [55]Y. Niimi, H. Suzuki, Y. Kawanishi, Y. Omori, T. Valet, A. Fert, and Y. Otani, Phys. Rev. B. **89**,
40 054401 (2014).

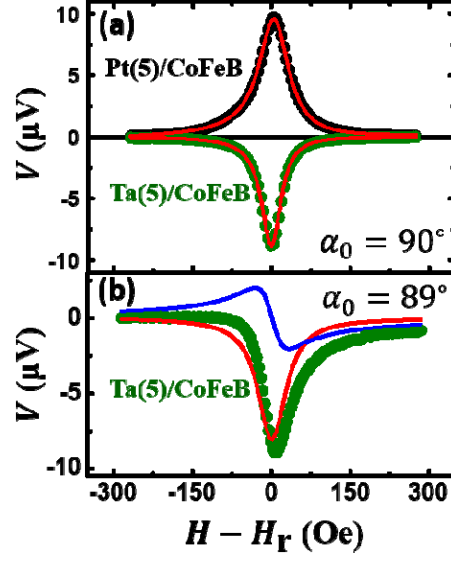
41



1

2 FIG.1. (a) Schematic illustration of the experimental setup for the spin pumping-induced ISHE
 3 voltage measurement. The Ta/CoFeB bilayer is placed in the middle of the gap between the ground
 4 (G) and signal (S) lines of a coplanar waveguide. (b) Schematic illustration of spin current
 5 transmission across the interface (I) between ferromagnetic (F) and normal (N) layer without
 6 considering interface spin loss (left) and with the interface spin loss (right).

7



1

2 FIG.2. (a) The measured voltage as the function of the external dc magnetic field, \vec{H} . The green
 3 solid symbols are for Ta (5)/CoFeB (10) and the black solid symbols are for Pt (5)/CoFeB (10),
 4 respectively. The data are obtained with $f = 8$ GHz and $\alpha_0 = 90^\circ$. The red lines are the fits utilizing
 5 the symmetrical Lorentzian function. (b) The measured voltage as a function of the external dc
 6 magnetic field \vec{H} for Ta(5)/CoFeB (10) at $f = 10$ GHz under $\alpha_0 = 89^\circ$. Symbols are the
 7 experimental data. The solid red/blue lines are the fits with the symmetrical/anti-symmetrical
 8 Lorentzian functions, respectively.

9

10

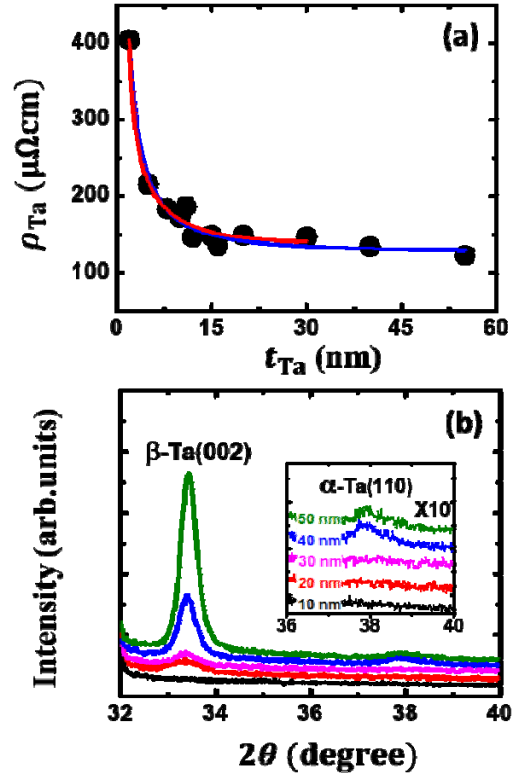
11

12

13

1

2

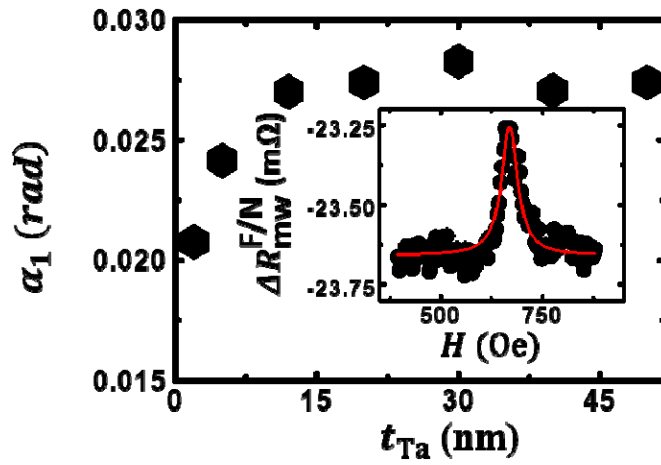


3 FIG. 3 (a) The Ta thickness dependent resistivity. Symbols are the experimental data, and the red

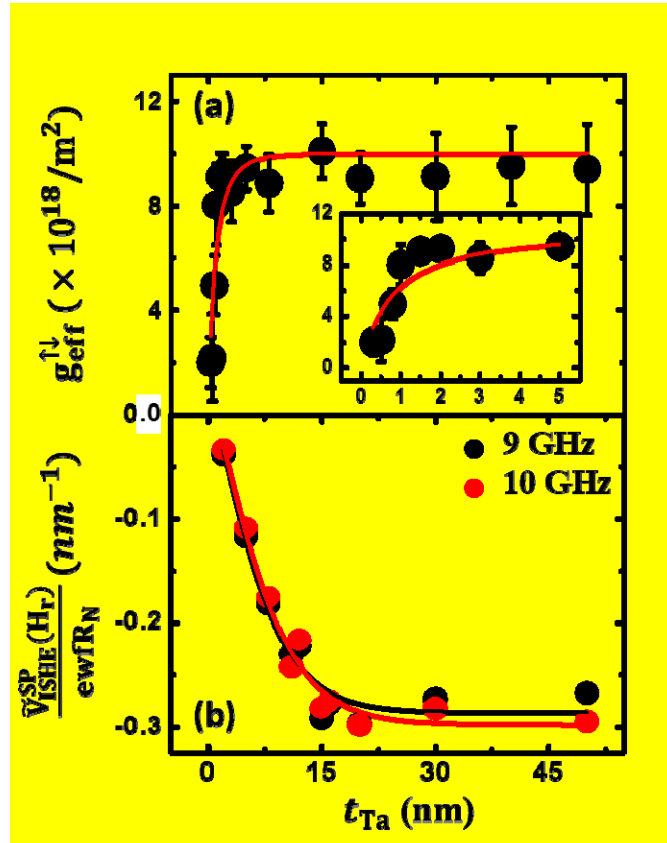
4 line is a fit using the Fuchs-Sondheimer model. (b) $\theta - 2\theta$ XRD scan of Ta (10/20/30/40/50) films

5 deposited on GaAs substrates. Inset shows the amplified view.

6



1
 2 FIG. 4. In-plane precession angle as a function of the Ta thickness. The inset shows a typical
 3 microwave photo-resistance signal used for the estimation of the in-plane precession angle. The
 4 signal was obtained with $\alpha_0 = 90^\circ$ and $f = 10$ GHz for Ta(20)/CoFeB(10).



1

2 FIG.5. (a) Ta thickness dependence of the effective spin mixing conductance. The solid line is the fit
 3 according to Eq. (1). The inset shows the effective spin mixing conductance as the function of the Ta
 4 thickness in the range of 0-5 nm. (b) Ta thickness dependence of ISHE signal measured at 9 GHz
 5 (black squares) and 10 GHz (red circle), respectively. The solid lines are the fits utilizing Eq. (2).